Segmentation and characteristic extraction for Schumann Resonance transient events★

ARTICLE INFO

Keywords:
Schumann Resonance
Extreme Low Frequency
Segmentation
lightning Activity
Narrow Band Sensor
Electro-Magnetic Signal Analysis

ABSTRACT

In this article we propose a novel methodology for obtaining Schumann Resonances' relevant parameters from ELF transient register. Using this methodology, it is possible to extract a large amount of data and characterize individual transient events and their more relevant features. To use this methodology a new narrow band sensor is presented, centered in the 1st Schumann Resonance mode and specialized in capturing with high precision the associated transient events. The new methodology based on Hilbert transform and Heidler function is presented and used to segment and characterize each transient event. This method is validated first with an automatic classifier algorithm and then an extensive statistical analysis is performed. The validation process is shown as one of the possible applications of the methodology. The introduced set of narrow band hardware and software tools represents an important milestone for the study of transient events focused on a high amount of data.

1. Introduction

*Schumann Resonance*s (SRs) are electromagnetic waves formed in the natural Earth-ionosphere cavity located in the *Extremely Low Frequency* (ELF) band, from 1 Hz to 100 Hz (Schumann [1952]). Global lightning activity has been established as the principal contributor to the resonances' electromagnetic energy (Ogawa et al. [1969]), whose strokes induce a strong electromagnetic disturbance that propagates along the atmosphere (Nickolaenko [2014]). The geometry and electromagnetic composition of the cavity determine its resonant frequencies (Tran and Polk [1979]). Many studies have been proposed to study the conductivity profile of the upper boundary of the cavity, both from a theoretical point of view (Kudintseva et al. [2018], Perotoni [2018]) and with a simulation approach (Goncharov et al. [2019], Kwisanga and Fourie [2017]).

Obtaining spectral information about SR and their associated natural phenomena is the typical methodology to study them, the reason why it has been widely addressed and is still the mainstream method of analysis. In Galuk et al. [2020], the authors proposed a model treatment for exploring the relationship between earthquakes and the modification of the SR's spectra, using a theoretical approach. The long-term variations are a popular subject of study (Koloskov et al. [2020], Bozóki et al. [2021]), where the goal is usually to experimentally prove the relationship between SRs and some natural phenomenon, relying on monitoring by two or more stations in different parts of the globe. Other authors are also interested in the frequency of regular variations either using one station (Anonymous et al. [2021]) or many (Tatsis et al. [2020]), without any particular focus on finding a connection with a specific event. Although spectral analysis is the most common approach for studying SR, a few studies rely on temporal registers to analyze the Earth-ionosphere signals (Anonymous et al. [2021]). Nonetheless, time-based methods are still in the minority.

The footprint of the global lightning activity on the spectrum is considered as the most critical phenomenon among ELF transient activity (Price [2016], Greenberg and Price [2007], Hobara et al. [2001]). For the most relevant events in ELF, a classification was proposed by Ogawa in 1966 (Ogawa et al. [1966]).

- ELF-Flashes: High amplitude transients caused by the strong interaction with a close lightning discharge, recognized by the receiver saturated response.
- Q-bursts: Short transient events associated with a powerful lightning discharge that resonates several times around the globe (Nickolaenko [2014]), with an average rate of one per minute.
- ELF background noise: It is the ELF register's base signal due to the continuous discharges all over the Earth.

An example of a Q-burst and background noise can be seen in Fig. 1a. Q-bursts are identified based on the total contribution in *Power Spectral Density* (PSD); when the register is above an absolute value, it is classified as a Q-burst (Guha et al. [2017]). Guided by the value extracted from the previous reference, any event with a peak value higher than 2×10^6 pT could be identified as a Q-burst. 29 events identified as Q-burst were detected with the method developed by the previously mentioned research in the validation segment.

Among the phenomena listed on this classification, Q-bursts are the only ones that can be considered transient events and, at the same time, generate data to be researched. This reason is why most ELF transient event studies are focused on them. Boccippio et al. [1995] proposed a first step in the identification between Q-bursts and *Transient Luminous Events* (TLE). This first approach is based on a few observations and the individual analysis of each transient event. The next milestone on this topic was published in Guha et al. [2017]. The authors explore the relation between Q-bursts and the TLEs known as Sprites. They used two long-distant ELF and a TLE optical sensors. This approach also focused on studying high peaks in the ELF register individually. The relation between TLE, always associated with

ORCID(s):

a *Positive cloud-to-ground* (CG+) discharge, and ELF events has been established (Inan et al. [2010], Pasko et al. [2012], Williams et al. [2007]). Specifically,There are three works that have been carried out on the potential association between Sprites and strong Q-bursts (Fukunishi et al. [1996], Haldoupis et al. [2010], Surkov and Hayakawa [2020]). However, some aspects of this relationship remain unexplained.

On the other hand, little to no attention has been given to the individual contribution of standard lightning events to the ELF spectrum. It is a widely stated fact that SR radio signal is the aggregated effect of many individual pulses coming from global lightning activity (Nickolaenko [2014]). It is also acknowledged that powerful lightning discharges generate a specific pattern in the time domain; the previously mentioned Q-bursts. When putting both facts together, it seems logical being able to find a typical time domain pattern in SR transient events that is directly related with lightning events.

Creating an automated methodology to identify and classify the contribution of these individual pulses is the goal of this paper. With that purpose in mind, a *Narrow-Band Extremely Low Frequency* (NB-ELF) sensor has been developed, featuring a band pass profile and centered in the first SR mode (7.8 Hz), which contains the most spectral information of the phenomenon. The previously mentioned studies about Q-bursts, performed using broadband sensors, show how these transient events are most present in this frequency band. This result leads to the assumption that by restricting the sensor band to the first mode, transient events should still be present and, since the rest of the frequencies are filtered, their presence should be more noticeable. A novel methodology for the segmentation and feature extraction of ELF transient register has been developed and presented here. It has been developed having in mind the new technologies for the treatment of a large amount of data, such as Deep Learning or Big Data since these can be successfully applied to a long time SR register and find day-to-day patterns, seasonal differences or yearly changes. The automatization purpose is another reason to restrict the sensor's frequency band to the first mode. Knowing the average frequency of the captured signal beforehand simplifies some steps of the automatic classification, such as envelope extraction.

The paper is organized as follows. Section 2 gives a brief overview of the studies published about lightning activity and ELF transient events. The new narrowband ELF sensor and the methodology developed are presented in section 3 with the algorithm used to extract the ELF transient events. The validation process is shown in the Results section 5 with particular emphasis on the relation between groups of transient events, followed by a discussion about the exposed result. Finally, conclusions are drawn in the final section.

2. Electromagnetic Interaction: Lightning, Ionosphere and ELF Band

The starting point for this methodology is the fact that most ELF transient events are created by lightning discharge. Therefore, the recorded waveform in the ELF register is the lightning discharge signal convoluted with the impulse response of the Earth-ionosphere waveguide (propagation effect) and further convoluted with the impulse response of the sensor stage. This paper is based on the assumption that the Earth-ionosphere lightning response is proportional to the charge distribution of the lightning, albeit extended in time due to the propagation and absorption characteristics of the medium at its eigenfrequencies. This hypothesis is supported by the typical behavior of impulse-generated signals in any resonant system concerning fading times. Specifically, the transient events already analyzed in the literature. Powerful Q-bursts rise to their peak value almost instantly, and from there on, the signal amplitude decays exponentially, in the same fashion as lightning releases their charge.

Nonetheless, the discrepancies between lightning discharge and electromagnetic resonance must be acknowledged; the anisotropy and variability of the resonant cavity will modify the response accordingly. It has to be taken in consideration as well that the resonant waves travel over the poles and across the day-night termination. All these causes general effects that prevents the determination of a single frequency, like mode splitting Labendz [1998]. Regarding the capture of transient events specifically, it leads to a peak time depending on the distance to the lightning perturbation. However, assign the peak value to the lighting peak current or determine the distance to the source from the analysis' results is outside the scope of this research.

By following that train of thought, it can be stated that by understanding the characteristics of the natural source - lightning discharges - we can study its effects on the ELF register. The outlined relationship gives way to the hypothesis of every noticeable amplitude variation in the ELF signal being the consequence of a specific electromagnetic transient event which, as stated before, is the goal of this paper. This relationship is in line with the literature, where papers can be found proving the relationship between ELF events and lightning activity Ramarao and Chandrasekaran [2020], Bermudez et al. [2007].

Through the hypothesis exposed before, The relevant time parameters for ELF transients can be extracted from the behavior of individual lightning discharges. The most relevant parameters for lightning discharges are:

- Rise time: Rise time is calculated as the time difference between the moment current reaches ten % and 90 % of its maximum discharge value. Experimental data shows average values ranging from 2 μs Wooi et al. [2019] to 5.6 μs (Visacro et al. [2004]).
- *Full Width at Half Maximum* (FWHM): The time measured between the points where the signal has a 50 % of its maximum value, which happens first in the rising part of the discharge the other in the falling part. Average values has been established experimentally from 23.8 μs (Wooi et al. [2019]) to 53.5 μs (Visacro et al. [2004]).
- Peak Current: There is considerable consensus about

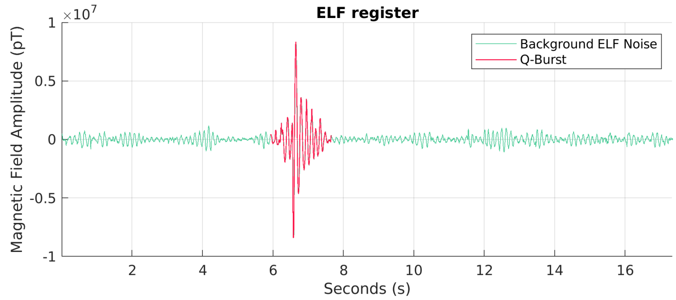

(a)

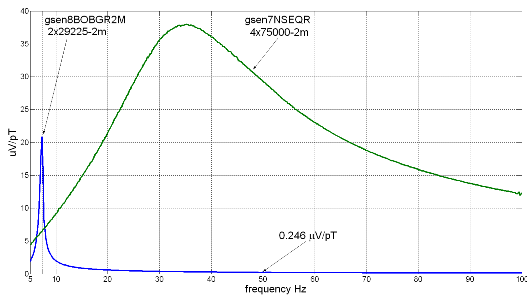

(b)

(c)

Figure 1: Sensor Characterization: a: Transient register with NB Sensor ELF background noise (Green Line) and Q-burst (Red Line), b: Frequency Response of the Broad Band Sensor - gsen7NSEQR (Green Line) and NB-ELF Sensor - gsen8B0BGR2M (Blue Line) and c: Physical implementation of the NB-ELF sensor.

peak current being modeled by log-normal distributions, widely demonstrated in Slyunyaev et al. [2018] This distribution has been also obtained experimentally (Almeida et al. [2012]) with a 15 % peak probability for 50 kA. High current discharges are usually modeled by a separate log-normal distribution, with peak values of 100 kA at 7 % probability (Chen et al. [2008], Jerauld et al. [2005]). Among the different kinds of electric discharges, CG+ are by far more powerful and infrequent than *Negative cloud-to-ground* (CG-), with peak current, discharges over 250 kA.

Another parameter that is relevant to define this relationship is the propagation effect of the Earth-ionosphere cavity. It has been studied using Sprites as a reference. Sprites are TLEs associated with strong discharges in the mesosphere. The majority of Sprites last few µs and the corresponding ELF perturbation last around 1 s (Soula et al. [2015]). So the propagation ELF event lasts 100000 times more than their corresponded generated lightning discharge.

This behavior is directly inferred from the fact that significant electromagnetic disturbances (Q-bursts) propagate through the Earth-ionosphere cavity, which takes $1/7.8$ s around eight times before it fades. This fading effect leads to an average duration of 1 s. If this is considered the cavity's impulse response, a similar response could be expected from isolated, non-Q-burst lightning events.

3. Sensor Design

The ELF band has been one of the fields of study for our research group in the last few years. Our group has done the design and implementation of a functional ELF observatory. This ELF observatory is able to record electromagnetic signals from 1 Hz to 100 Hz for $\mathcal{H}_{NS}$ and $\mathcal{H}_{EW}$ orientations. A complete description of the functionality can be seen in [AnonimousRef]. This observatory was designed to obtain the maximum possible characteristics of the SRs up to the 6th mode, around 45 Hz. However, specific transient events are hardly distinguishable in the time domain due to the broadband sensor response, a limitation experienced by all broadband sensors.

Previous works were focused on obtaining the maximum spectral power information for the study of Schumann Resonances using a broadband sensor that can capture the maximum number of SR modes. Due to its broadband characteristics, these sensors capture all modes of SR which is vital to study the signal as a whole. They also capture other signals in the same range such as power lines or trains interference (16.6 Hz and 50 Hz, respectively), usually filtered out by digital means. That being said, to study SR transient events, this kind of strategy falls short. The interferences caused by other signals mask the effect transient events may have on the records, as well as the presence of the other modes. Digital filtering could be a solution, but it comes with a tradeoff in signal resolution, which is paramount for this study. We have studied and analyzed the data obtained by our broadband ELF observatory and reached the conclusion that the significant important part of the transient information is centered around the 1st SR mode. Following this line, we have developed a specific bandpass sensor with a narrow band profile and a central frequency of 7.8 Hz (NB-ELF). The sensing coil's features a Nylomag 77 core with a diameter of 45 mm and longitude of 2 m. The coil's longitude is 0.7 m, with a total diameter of 230 mm. A nylon bobbin supports the winding, and it is done using copper wire of 0.92 mm including the insulating layer, with a total of 57000 turns distributed in 75 layers. This sensor's ELF records show amplitude variations that don't feature in the ones produced by broad band sensors. These amplitude variations fit the expectations of finding additional transient events, and they are measured with a tiny part of noise in comparison with the broadband sensor. Concerning the band of interest for our purpose, around d7.8 Hz, the peak magnetic induction of the sensor as a function of frequency is 20 µV pT^{-1}.

In other words, sensing the electromagnetic field with a sensor focused on the average central frequency of the first mode allows us to widen the system's response to extract the transient events with the highest possible resolution. The frequency comparison between the NB-ELF sensor and the one installed in the observatory mentioned above can be observed in Fig. 1b.

The preliminary tests with the NB-ELF sensor showed transient effects identifiable by a visual inspection. These had enough amplitude variation over time to be differentiated from ELF background noise but not enough to be considered a Q-burst.

For this study, different measurements were taken with the described sensor and some portable acquisition equipment, collecting data from the $\mathcal{H}_{EW}$ axis of the magnetic field. The sensor was deployed on the selected location and supported on two stands, specifically designed for this purpose. Data was stored locally on a computer in fifteen minutes' files. Due to wind presence affecting measurements, we have selected a register with the lowest disturbances. For this purpose, the measurement lengths 15 minutes and was performed in a completed isolated place without any possible human interference in Location remove due to the anonymization process. An image of the physical implementation of the sensor can be seen in Fig. 1c.

4. Methodology

The observations mentioned above contain some transient signal events of Q-bursts and ELF background noise, measurable in the frequency band of the first SR mode with our sensor. This research aims to design a methodology for the segmentation and feature extraction of ELF transient events, allowing us to study their most relevant features. As the literature characterization of the ELF, transient events are exclusive of the Q-burstas the only type of ELF events, we have studied this type of events in our registers to develop this tool. Then, the identification method will be applied to the rest of identified transient events under the assumption that they share lightning activity as their source. Lastly, the extracted parameters for each transient event will allow the validation through an automatic classification and a statistical comparison.

The complete methodology used through this research can be seen in Fig. 2.

In order to show an application of the proposed methodology, we have applied it on a NB-ELF register, with a time duration of fifteen minutes.

Stage 1: Hilbert Process

The first step to study transient events in the time domain through this research is extracting the envelope from the original register (Fig. 3). The need for envelope detection is based on the assumption that the central frequency is not constant, so an instantaneous frequency must be estimated for each identified event. The one that yielded the best results was the envelope detection process based on the Hilbert transform Brandwood [2013]. This method has been widely used in different fields, such as mechanical vibration and power grids. Briefly, the process consists on applying the Hilbert transform (Eq.1) to the original signal $x_s(t)$ to obtain the analytical signal $\hat{x}_s(t)$. Therefore, the amplitude is calculated using Eq. 2, in which v_s is the envelope signal. Lastly, the register is downsampled with a factor of two, and an optimal low pass filter with a cutoff frequency of 3 Hz is applied. The process to extract the envelope can be seen in Fig. 3a. From the left column, it can be observed that all the information around 7.8 Hz (at baseband) is preserved along with the Hilbert transform. The spectral information can be observed in the right column. It shows that the Hilbert algorithm is able to preserve the majority of the information in the first resonant, moved to 0 Hz due to the envelope detection process.

$$\hat{x}_s(t) = \frac{1}{\pi t} * x_s(t) = \frac{1}{\pi} \int_{-\infty}^{\infty} \frac{x_s(\tau)}{t-\tau} d\tau \tag{1}$$

$$v(s) = \sqrt{\left|x_s^2\right| + \left|\hat{x}_s^2\right|} \tag{2}$$

Stage 2: Segmentation

At this stage, the process of identifying separate transient events is done by the fitting procedure. It focuses on finding signal peaks, considering it the most representative value of each ELF transient event. Obtaining the peak value is a processing algorithm that aggregates and weights the difference with previous and next peaks, peak prominence, the absolute value itself, and the separation between peaks. A transient event is narrowed down for each peak found by extracting its starting and ending points from local minima. Acquiring the boundary points of a transient event consists of evaluating all the relative minima within a specific range of the peak and choosing the most likely segmentation by using the distance to the point and the prominence of the value itself. An example of this stage can be seen in Fig. 3b.

Stage 3: Heidler Fit

Up to this point, different segments are identified in the registers. Some of these segments can be classified as Q-bursts according to the definition in the literature Boccippio et al. [1995]. A process for modeling the envelope of the Q-burst ELF events has been applied, using fitting and cross-validation. In the last few years, the Heidler function has been used as an analytical interpretation of lightning discharges, being included in the IEC 62305 standard (Heidler

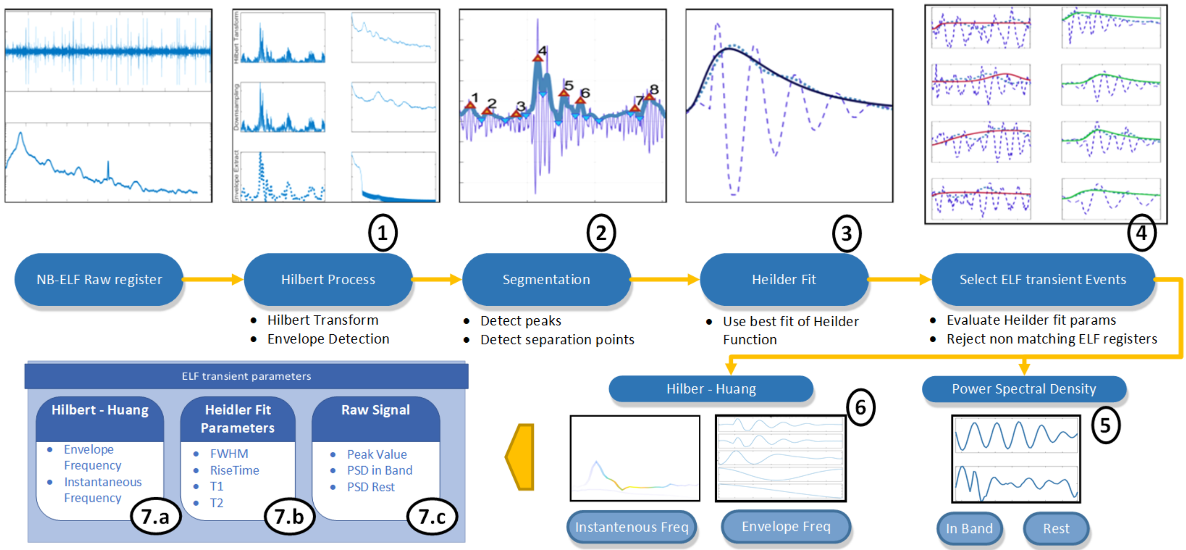

Figure 2: Methodology Flow diagram.

and Cvetić [2002]). Two parts compose the Heidler function, each corresponding to a separate phase of the natural discharge.

The Heidler function can be seen in Eq. 3, where $x(t)$ is the rise equation (Eq. 4) and $y(t)$ the fall equation (Eq. 5).

$$i(t) = \frac{I_o}{\eta} x(t) y(t) \tag{3}$$

$$x(t) = \frac{(t/\tau_1)^{nh}}{1 + (t/\tau_1)^{nh}} \tag{4}$$

$$y(t) = exp(-\frac{t}{\tau_2}) \tag{5}$$

The variables take the following meaning:

- I_o: Current peak value.
- η: Correction factor for the peak current.
- τ_1: Model fit rise time.
- τ_2: Model fit fall time.
- nh: Current steepness factor.

The graphical representation and its most representative parameters can be seen in Heidler and Cvetić [2002].

Following the hypothesis at the start of the section, if Q-burst can be modeled as a Heidler function, it will acceptably fit the rest of the ELF transient events, assuming that both have the same origin. Then, it is possible to extract valuable parameters from the model of both types of events. An example of segment fit can be observed in Fig. 3c.

Stage 4: Select individual ELF Transient Events

ELF transient events are hard to identify in some cases due to the nature of the phenomena. There is not just one isolated phenomenon in multiple cases, and it is not possible to simultaneously identify a Heidler function with multiple transient events. For this reason, the next layer of the algorithm is to classify and reject segments that do not meet the criteria of the response to an isolated natural phenomenon. As mentioned before, to choose the criteria, information about lightning discharges has been considered. The specific thresholds for these criteria are related to the natural phenomenon studied, and to fine tune them, we have relied on visual inspection of the results through several iterations. In the end, they were set up in a conservative way to prevent false positives, even if the number of transient events captured is not as high as it can be. For example, the ratio between fall time and rise time can not be greater than 20, and rise time cannot be shorter than one signal period, due to the sensor's sensitivity. The criteria used are based on the following aspects

- Fitting error.
- Ratio between FWHM and rise time.
- Ratio between fall time and rise time.
- Ratio between rise time and the period of the first resonance $\frac{1}{7.8\,\mathrm{s}}$.
- Ratio between FWHM and the period of the first resonance $\frac{1}{7.8\,\mathrm{s}}$.
- Envelope instant frequency value.
- Carrier instant frequency value.

Stage 5: Power Spectral Density (PSD)

Using the Heidler function fitting process, some characteristics of the transient events are extracted. Moreover, other interesting parameters can be obtained from the raw signal, so a signal analysis is performed directly to each ELF transient event's raw signal. The sum of the PSD of the 1st SR and the sum of the PSD in the rest of the spectrum are obtained using an averaging process of the spectral information in

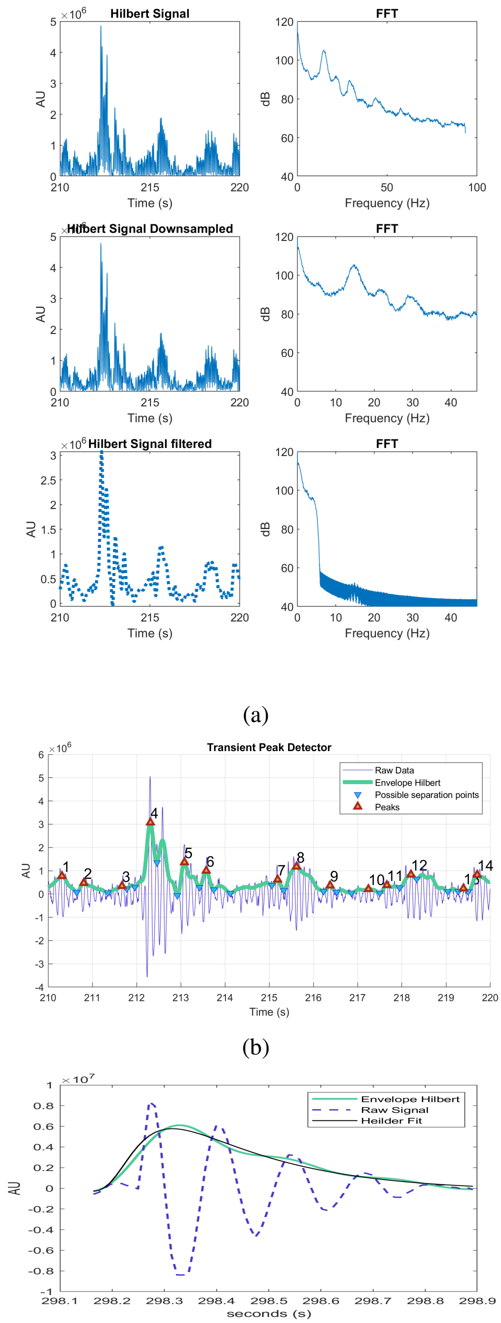

(a) (b) (c)

Figure 3: Process for extracting ELF transient events a: Envelope detection algorithm in time domain (Left Column) and Frequency domain (Right Column), b: Segmentation of ELF transient events and c: Fit of ELF transient segment.

each segment. The parameters show the importance of the PSD around 7.8 Hz when a relevant ELF transient event is captured.

Stage 6: Hilbert - Huang transform

The premise of the signal under study having no constant frequency can be confirmed by inspecting the frequency spectrum of the signal (Fig. 4a), which is a broadband signal.

To analyze the changes of the broadband signal, the Hilbert-Huang transform (Bowman and Lees [2013]) has been used. It decomposes the signal in its intrinsic mode functions and compares the instantaneous frequency of each decomposition with the segment peak value. The Huang algorithm addition to the Hilbert base allows the system to decompose the signal in the sum of different relevant signals known as intrinsic functions. The Hilbert algorithm can extract the instantaneous frequency in each of these functions. The decomposition can be seen in Fig.4b and the instantaneous frequency of the first intrinsic mode function of the same register in Fig.4c.

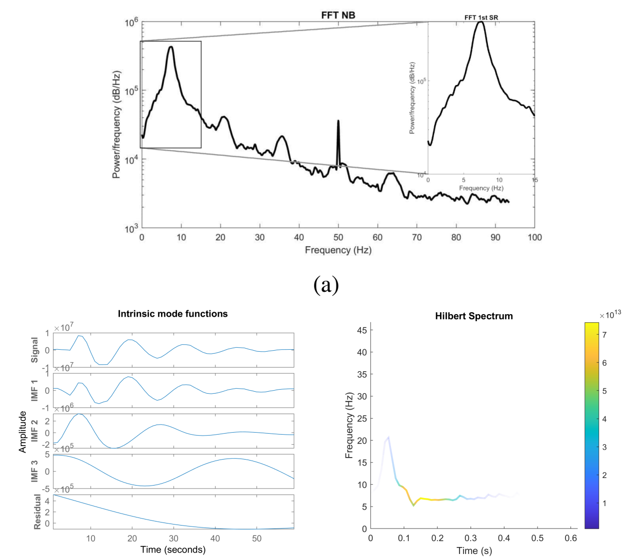

(a) (b) (c)

Figure 4: Process for extracting and classifying ELF transient events, a: Frequency transform of an NB-ELF register, b: Intrinsic mode functions, c: Instantaneous frequency of the first intrinsic mode function.

Stage 7: ELF transient Parameters

From this point on, the study is based on analyzing the individual registers obtained in the previous stage. This stage is focused on identifying and extracting the most useful parameters. The utility of each parameter is based on the ability to characterize the ELF transient event, either about its power, duration, or frequency.

Stage 7.a: Hilbert - Huang Parameters

Two valuable parameters can be extracted based on the Hilbert - Huang transform mentioned in the previous stage. First, the instantaneous frequency, being the most relevant. It is typically around 7.8 Hz, although it commonly varies when a powerful ELF event starts. The second parameter is the envelope frequency. It refers to the period of variation in the amplitude of each ELF event. This frequency contains valuable information about the event's magnitude in the time domain.

Stage 7.b: Heidler Fit Parameters

As we can see in Eq. 3, Heidler function has 5 parameters. In order to characterize the ELF transient events, only two of these parameters are considered for this analysis: τ_1 and τ_2. This reduction of variable size is important to diminish the complexity of the methodology and understand the relation between variables, although all possible variables could be taken into account. Using these two parameters as a baseline, it is possible to calculate two more: FWHM and rise time. These two additional parameters provide a more practical description of the ELF transient event behavior. τ_1, τ_2, FWHM, and rise time parameters are included in the following stages. It is relevant to note that the rise time variable differs from the τ_1 due to the latter is directly from the model fit (hence, model fit rise time), whereas the rise time is calculated based on the time between the signal is between the 10% and the 90% during the rising part.

Stage 7.c: Raw signal parameters

Although an envelope detection process has been applied before the segmentation, some parameters provide more helpful information without the signal processing method. The unprocessed signal absolute peak value and the PSD values around 7.8 Hz and in the rest of the band have been selected.

5. Results and Discussion

We have applied the implemented methodology to a data register of the NB-ELF sensor with the aim of validating both the sensor and the methodology.

The result of the methodology will be presented, following by a brief discussion about the main milestones reached.

5.1. Results

The validation process is split into two parts, automatic classification, and statistical comparison. As it was mentioned before, the data is collected in segments of fifteen minutes, For this validation purpose, we have analyzed one segment in which we have isolated 553 Events.

5.1.1. Automatic Classification

The algorithm has extracted four parameters from the Heidler fit stage (two from the fit process and two calculated), three from the raw signal stage, and two related to the Hilbert - Huang transform stage. This process separates high-power ELF transients from the rest of ELF transients using the mentioned parameters.

First, dimensionality reduction is made using the PCA algorithm (Husson et al. [2010]). This method is an orthogonal linear transformation that transposes data into a new coordinate system that preserves the majority of the information. These new data dimensions are a linear combination of the original ones. In this methodology, dimensions are reduced from 9 (one for each parameter) to 2, thus finding the two-dimensional plane among the data space the data is most spread out.

The last step of this layer uses an automatic classification algorithm to find the two categories with their means as close as possible (Lloyd [1982]). The technique employed is K-means, which is essentially a clustering approach related to unsupervised learning, but it can also be adapted to handle classification problems Kim and Gil [2019], Stoean et al. [2019]. The results can be seen in Fig. 5. The groups created by the classification algorithm are separable into the two most relevant reduced dimensions, as shown in Fig. 5a. Furthermore, when the two selected variables are peak value and band power, both groups are seemingly differentiated as well (Fig. 5b).

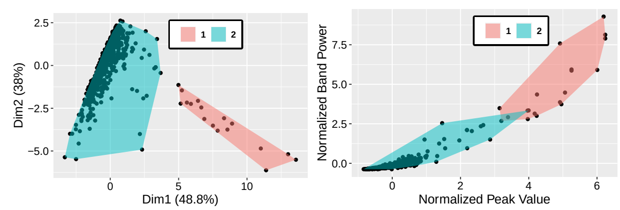

(a) (b)

Figure 5: Automatic classification, a: Adimensional view classification and b: Peak value-band power dimensional view classification.

5.1.2. Statistical Comparison

Statistical analysis will be applied to the variables of the extracted segments.

Lightning Discharges Comparison

There are a few statistical classifications of lightning activity in the literature. To further test the assumption of lightning activity being the source of the analyzed transient events, Akaike Information Criterion (AIC) was used to choose the distribution that best describes the histogram representation of the parameters of each segment. This result is helpful in order to study natural excitation.

The most relevant parameters of a discharge are related to the current and the duration. In Fig. 6 one can see the distribution of related parameters in the ELF transient event.

Under this method, it can be determined that Fig. 6a finds its best fit in a log-normal distribution with a mean value of 0.6386 µT and a *Standard Deviation* (SD) of 0.34 µT.

Rise time histogram can be seen in Fig. 6b, which is also best fitted by the log-normal distribution, with the parameters of the distribution are a mean of 0.2435 s and a SD of 0.125 s.

The SR frequency spectrum is composed of the ELF transient event, which has more power in the band of the 1st SR (7.8 Hz). In Fig. 6c the distribution of the accumulated power in the band is presented. The most likely theoretical distribution using AIC is once again log-normal, and its resulting parameters are a mean of 2.23×10^9 pT and an SD of 0.3×10^9 pT.

Correlation Comparison

Fig. 7a shows the correlation between the peak value of the ELF transient event and their correspondent band power in the 1st SR band. The high correlation between the two can be observed with a strong dependency with $y \propto x^2$. Fitting with a quadratic function, the result shows a regression

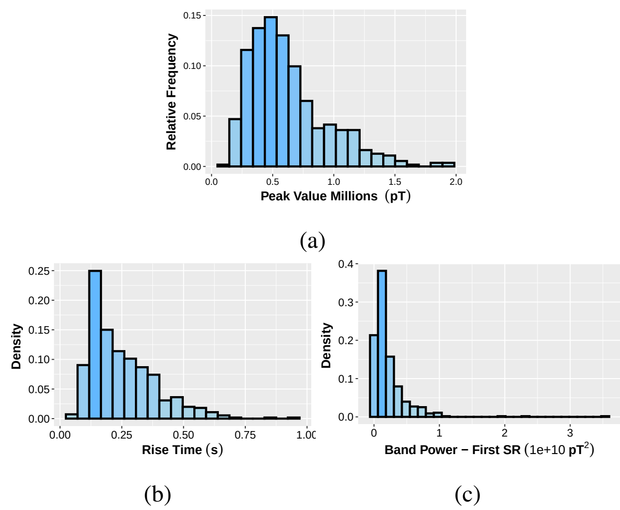

Figure 6: Distribution of relevant parameters without high peak samples. a: Peak value, b: Rise time and c: Band power 1st SR.

coefficient of $R^2 = 0.95$. On the other hand Fig. 7b correlates peak value with power over the rest of the band with an still high $R^2 = 0.88$. A high correlation was to be expected in both cases, since the peak value of a transient event is directly related with its power. The point of this correlation is to show how, by considering only the first mode of the SR, the correlation improves and dispersion is reduced. In other words, it serves as further validation of the approach of studying these transient events by means of the first SR mode.

It is noticeable that the difference in the lower values of the x-axis does not follow a clear tendency. In the same way high peak values are more dispersed than the band power in the 1st SR.

Distributions Comparison

The critical parameters of each ELF transient event are compared against the peak value in Fig. 8. The peak value of a selected segment represents the amplitude of the transient event with high precision. In each graph, the red dots represent ELF transient events classified as non Q-bursts, while blue dots are classified as Q-burst. In all figures, the x-axis is the peak value. In Fig. 8a it is selected the FWHM related to the duration of the whole event. It is possible to distinguish that Q-bursts and non Q-bursts events are distributed similarly without any clear tendency. Rise time is present in Fig. 8b. We can see that Q-bursts are more likely distributed with rapid values of rise time, although non Q-burst are also present in the lower values of the time.

The instantaneous frequency presented in section 4 is used to extract the period's average frequency under analysis. The supposition is that transient events are determined to construct the complete SR spectrum, and the instantaneous frequency could identify a change in the frequency in short times as the duration of the event. The distribution of these parameters concerning the peak value can be seen in Fig. 8c. It is clear that Q-burst events are less dispersed than

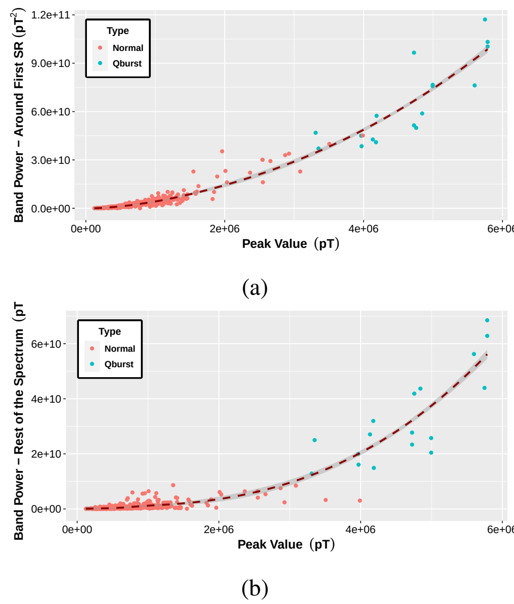

Figure 7: Relation between peak value and band power: a: Band power in the band of the 1st SR resonance and b: Band power in the rest of the spectrum.

non-Q-burst events. However, it is under the same range of values.

Envelope frequency is a concept related to a broadband signal that is considered a frequency that determines the envelope shape. The envelope frequency is shown in Fig. 8d. There is a clear tendency for Q-burst events to be highly situated in the lowest part of the frequency, while the non-Q-burst events are widely spread but with a slight focus on the lower values.

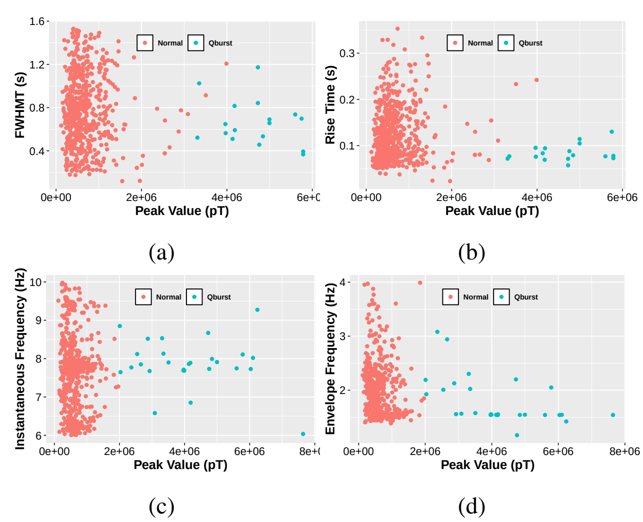

Figure 8: Distribution of key parameters for non Q-burst (red dots) and Q-burst (blue dots). a: FWHM, b: Rise time, c: Instantaneous Frequency and d: Envelope Frequency.

Quantile Comparison

Through quantile comparison it is possible to observe if data density distribution is similar even when the scale is entirely different. If the points are close to the $y = x$ curve, the distribution density between both parameters is similar. The classification applied to the tested segment identifies 19 segments as Q-burst and 526 as non-Q-burst. Applying the techniques mentioned in the last part of the previous section, the differences and similarities between these two segment groups will be presented.

In Fig. 9, a comparison between the percentile distribution of the most critical parameters from each group of ELF transient events are shown. Statistical differences between the Q-burst and rest of the transient events can be seen in the case of band power (Fig. 9a) and Peak value (Fig. 9b). On the other hand, Envelope Frequency (Fig. 9c) and rise time (Fig. 9d), are more concentrated in the case of Q-burst. However, it is considerably surprising that in the instantaneous frequency (Fig. 9e), and FWHMT (Fig. 9f), the distributions show a common behavior with values close to the $y = x$ line. This points out how low powered transient events have a behavior which is similar to Q-bursts, but smaller in amplitude. This gives evidence to the hypothesis of other lightning (not only high discharges) leaving traces in the ELF spectrum.

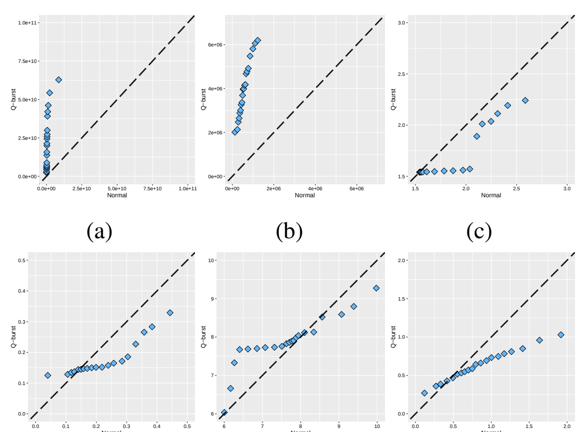

(a) (b) (c)

(d) (e) (f)

Figure 9: Comparison of the percentile distribution of the key parameters between Q-burst and Normal transient events though qq-plots.a: Band power in 1st SR, b: Peak value, c: Envelope frequency, d: Rise time, e: Instantaneous frequency and f: FWHM.

5.2. Discussion

The previous results are consistent with the known facts of the SRs, and also support the hypotheses explained in the first sections of the article. They are good evidence of the methodology performance, making the segmentation process and parameters extraction a promising feature to the study of ELF transient events. In the scope of this paper, it is directly related to the identified transient events, but also the amount of generated data by the methodology gives way to study them further by using deep learning methods.

The classification presents a substantial difference over the standard deviation method (Guha et al. [2017]) on analyzed data using NB-ELF. When using the automatic classification after applying the segmentation and feature extraction methodology with the 15 min of the NB-ELF register, the method identifies 19 transient events as Q-burst. On the contrary, the SD method identifies 29 Q-burst.

The result using the technique proposed in this article $1.27\,\frac{\text{Q−burst}}{\text{min}}$ is more consistent with the accepted ratio of $1\,\frac{\text{Q−burst}}{\text{min}}$ than with the SD technique $1.93\,\frac{\text{Q−burst}}{\text{min}}$.

An important marked observation to emerge from the data comparison was that the distribution of peak value from the regular transient events follows a log-normal distribution, which models the lightning peak current as well (Herrera-Murcia et al. [2017]). This result offers evidence in favor of the close relationship between the lightning discharge peak current and transient event peak value (Salut et al. [2013], Arshad et al. [2020]).

Our experiments are in line with the previous findings in the literature about lightning discharges times (Wooi et al. [2019], Heidler and Paul [2020], Wu et al. [2020]). The lightning discharge distribution shows a similar signal waveform as shown in Fig. 6b. The Lightning discharge duration is around 10000 times larger than the ELF transient events. This difference is manly due to the propagation characteristics of the ionosphere.

The high correlation between the peak value and band power in the 1st SR mode is noteworthy because it shows evidence that the most significant contribution of the transient event belongs to this band. This fact is more so since the correlation using the rest of the spectrum shows lower values. Interestingly, it is noticeable for Q-bursts and evident for the rest of transient events. This correlation endorses the hypothesis that every ELF transient event contributes to some extent to the complete SR spectrum, as is indicated in other research (Pizzuti et al. [2021]).

Considering the above, the distribution of the parameters shown in Fig. 8 is very similar between Q-burst and the rest of the transient events. The dispersion shown is wider in the rest of the ELF transient events than in the Q-burst. These differences can partly be explained by the aliasing caused by the overlap of various transient events of low peak value within the same register. Q-burst events are less susceptible to this phenomenon due to their high peak value, making it very difficult for overlapped transient events to be noticeable. This difference lends support to the hypothesis that Q-bursts and the rest of the ELF transient events proceed from the same natural phenomena, in line with the literature (Boldi et al. [2018], Prácser et al. [2019], Pracser et al. [2020]).

In the direct comparison of the obtained parameters (Fig. 9) between Q-burst and non-Q-burst ELF transient events, the following could be observed: As expected, the values of band power in the 1st SR mode and peak value are significantly reduced in the case of non-Q-burst events. The explanation lies in the nature of the Q-burst, related to high power lightning discharge. On the other hand, Envelope Frequency and rise time show higher dispersion in non-Q-bursts than in Q-bursts. The nature of the register points to overlapping as the source of this dispersion, although it is hard to provide a conclusive explanation for these values given the limitations mentioned above. All the transient events contribute to form the 1st

SR as it can be extracted from Fig. 8c. However, Q-burst events are more concentrated to the theoretical value 7.8 Hz. It could be explained by the power of these ELF transient events, which can propagate entirely more times than other ELF transient events (Ogawa and Komatsu [2007]).

FWHM is the only measurement that considers both the peak value and the duration of the ELF transient event, making this parameter the most relevant one. To stress the relevance of this parameter, Fig. 9f shows a strong high tendency between Q-bursts and non-Q-bursts. This result offers compelling evidence for ensuring that all the analyzed ELF transient events contribute on their own to the SR signal. Hence, Q-burst events are just the most potent evidence of lightning discharges on the ELF register. Despite that, other lightning transient events exposed in section 2 are also measurable with an appropriate sensor such as the NB-ELF.

All these results reinforce how this methodology, along with a narrow band sensor, can produce vast amounts of data, which can apply deep learning methods. In turn, this may allow finding common patterns with other phenomena or evaluating ELF transient events' self-variability.

6. Conclusions

To sum up, this paper presents a novel methodology to identify transient events in the ELF time signals and to characterize each by extracting its most relevant features. Transient event identification is complemented with the design of a narrow band sensor centered in the 1st mode of the Schumann Resonances, which enhances the signal-to-noise ratio capture of these events.

Through these tools, medium-low amplitude transient events have been identified in the ELF records, which despite being theorized, to the best of our knowledge, were never analyzed in detail. These transient events have been compared with the most studied ELF transient events (Q-bursts). A few specifics must be highlighted.

- The methodology successfully differentiates between Q-bursts and the other, more common transient events employing an automatic classification method.
- Nonetheless, the existing resemblances between the low amplitude transient events and those identified as Q-bursts point out how lightning discharges also produce the former.
- Furthermore, the number of identified transient events is consistent with the average estimate for lightning discharges per minute.
- To characterize each transient event, several different parameters are extracted. A tentative analysis of the importance of each parameter has been performed, with full width at half maximum being the most representative for the classification purpose.

Using this methodology over an extensive period, it is possible to obtain a large amount of data that can be processed using machine learning techniques or analysis. The segmentation and feature extraction methodology can be used for a variety of different applications, and mainly to understand the relation between ELF transient events and ionosphere parameters, such as solar flux or virtual height of the ionosphere.

References

W. O. Schumann. Über die strahlungslosen Eigenschwingungen einer leitenden Kugel, die von einer Luftschicht und einer Ionosphärenhülle umgeben ist. *Zeitschrift fur Naturforschung - Section A Journal of Physical Sciences*, 7(2):149–154, 1952. ISSN 18657109. doi: 10.1515/zna-1952-0202.

Toshio Ogawa, Yoshikazu Tanaka, and Michihiro Yasuhara. Schumann Resonances and Worldwide Thunderstorm Activity: Diurnal Variations of the Resonant Power of Natural Noises in the Earth-Ionosphere Cavity. *Journal of geomagnetism and geoelectricity*, 21(1):447–452, 1969. ISSN 00221392. doi: 10.5636/jgg.21.447.

Alexander Nickolaenko. *Resonance for Tyros*. 2014. ISBN 9784431543572.

A. Tran and C Polk. Schumann resonances and electrical conductivity of the atmosphere and lower ionosphere-II. Evaluation of conductivity profiles from experimental Schumann resonance data. *Journal of Atmospheric and Terrestrial Physics*, 41(12):1249–1261, 1979. ISSN 00219169. doi: 10.1016/0021-9169(79)90028-X.

I. G. Kudintseva, Yu P. Galuk, A. P. Nickolaenko, and M. Hayakawa. Modifications of Middle Atmosphere Conductivity During Sudden Ionospheric Disturbances Deduced From Changes of Schumann Resonance Peak Frequencies. *Radio Science*, 53(5):670–682, 2018. ISSN 1944799X. doi: 10.1029/2018RS006554.

Marcelo B Perotoni. Eigenmode prediction of the schumann resonances. *IEEE Antennas and Wireless Propagation Letters*, 17(6):942–945, 2018. ISSN 15361225. doi: 10.1109/LAWP.2018.2825398.

E. S. Goncharov, A. N. Lyakhov, and T. V. Loseva. 3D-FEM simulation model of the Earth-ionosphere cavity. *Journal of Electromagnetic Waves and Applications*, 33(6):734–742, 2019. ISSN 15693937. doi: 10.1080/09205071.2019.1575289.

Christian Kwisanga and Coenrad J. Fourie. 3-D modeling of electromagnetic wave propagation in the uniform earth-ionosphere cavity using a commercial FDTD software package. *IEEE Transactions on Antennas and Propagation*, 65(6):3275–3278, 2017. ISSN 0018926X. doi: 10.1109/TAP.2017.2695532.

Yuri P. Galuk, Irina G. Kudintseva, Alexander P. Nickolaenko, and Masashi Hayakawa. Modifications of Schumann resonance spectra as an estimate of causative earthquake magnitude: The model treatment. *Journal of Atmospheric and Solar-Terrestrial Physics*, 209(January):105392, 2020. ISSN 13646826. doi: 10.1016/j.jastp.2020.105392.

A. V. Koloskov, A. P. Nickolaenko, Yu M. Yampolsky, Chris Hall, and O. V. Budanov. Variations of global thunderstorm activity derived from the long-term Schumann resonance monitoring in the Antarctic and in the Arctic. *Journal of Atmospheric and Solar-Terrestrial Physics*, 201 (February):105231, 2020. ISSN 13646826. doi: 10.1016/j.jastp.2020.105231.

Tamás Bozóki, Gabriella Sátori, Earle Williams, Irina Mironova, Péter Steinbach, Emma C. Bland, Alexander Koloskov, Yuri M. Yampolski, Oleg V. Budanov, Mariusz Neska, Ashwini K. Sinha, Rahul Rawat, Mitsuteru Sato, Ciaran D. Beggan, Sergio Toledo-Redondo, Yakun Liu, and Robert Boldi. Solar cycle-modulated deformation of the earthionosphere cavity. *Frontiers in Earth Science*, 9:735, 2021. ISSN 2296-6463. doi: 10.3389/feart.2021.689127. URL https://www.frontiersin.org/article/10.3389/feart.2021.689127.

G. Tatsis, V. Christofilakis, S. K. Chronopoulos, G. Baldoumas, A. Sakkas, A. K. Paschalidou, P. Kassomenos, I. Petrou, P. Kostarakis, C. Repapis, and V. Tritakis. Study of the variations in the Schumann resonances parameters measured in a southern Mediterranean environment. *Science of the Total Environment*, 715, 2020. ISSN 18791026. doi: 10.1016/j.scitotenv.2020.136926.

Colin Price. ELF electromagnetic waves from lightning: The schumann resonances. *Atmosphere*, 7(9), 2016. ISSN 20734433. doi: 10.3390/atmos7090116.

Eran Greenberg and Colin Price. Diurnal variations of ELF transients and background noise in the Schumann resonance band. *Radio Science*, 42 (2):n/a–n/a, 2007. doi: 10.1029/2006rs003477.

Yasuhide Hobara, N. Iwasaki, T. Hayashida, M Hayakawa, K Ohta, and H Fukunishi. Interrelation between ELF transients and ionospheric disturnances in association with Sprites and Elves. *Geophysical Research Letters*, 28(5):935–938, 2001. ISSN 00948276. doi: 10.1029/2000GL003795.

Toshio Ogawa, Yoshikazu Tanaka, Teruo Miura, and Michihiro Yasuhara. Observations of Natural ELF and VLF Electromagnetic Noises by Using Ball Antennas. *Journal of geomagnetism and geoelectricity*, 18(4): 443–454, 1966. ISSN 00221392. doi: 10.5636/jgg.18.443.

Anirban Guha, Earle Williams, Robert Boldi, Gabriella Sátori, Tamás Nagy, József Bór, Joan Montanyà, and Pascal Ortega. Aliasing of the Schumann resonance background signal by sprite-associated Q-bursts. *Journal of Atmospheric and Solar-Terrestrial Physics*, 165-166(April):25–37, 2017. ISSN 13646826. doi: 10.1016/j.jastp.2017.11.003.

Dennis J Boccippio, Earle R Williams, Stan J Heckman, Walter A Lyons, Ian T Baker, and Robert Boldi. Sprites , Q-Bursts and Positive Ground Strokes. *Science*, 269(August):1088–1091, 1995.

U. S. Inan, S. A. Cummer, and R. A. Marshall. A survey of ELF and VLF research on lightning-ionosphere interactions and causative discharges. *Journal of Geophysical Research: Space Physics*, 115(6):1–21, 2010. ISSN 21699402. doi: 10.1029/2009JA014775.

Victor P. Pasko, Yoav Yair, and Cheng Ling Kuo. *Lightning related transient luminous events at high altitude in the earth's atmosphere: Phenomenology, mechanisms and effects*, volume 168. 2012. ISBN 1121401198. doi: 10.1007/s11214-011-9813-9.

E. R. Williams, V. C. Mushtak, R. Boldi, R. L. Dowden, and Z. I. Kawasaki. Sprite lightning heard round the world by Schumann resonance methods. *Radio Science*, 42(2):1–11, 2007. ISSN 00486604. doi: 10.1029/2006RS003498.

H. Fukunishi, Y. Takahashi, M. Kubota, K. Sakanoi, U. S. Inan, and W. A. Lyons. Elves: Lightning-induced transient luminous events in the lower ionosphere. *Geophysical Research Letters*, 23(16):2157–2160, 1996. doi: https://doi.org/10.1029/96GL01979.

C. Haldoupis, N. Amvrosiadi, B. R. T. Cotts, O. A. van der Velde, O. Chanrion, and T. Neubert. More evidence for a one-to-one correlation between Sprites and Early VLF perturbations . *Journal of Geophysical Research: Space Physics*, 115(A7):1–11, 2010. doi: 10.1029/2009ja015165.

Vadim V. Surkov and Masashi Hayakawa. Progress in the Study of Transient Luminous and Atmospheric Events: A Review. *Surveys in Geophysics*, 41(5):1101–1142, 2020. ISSN 15730956. doi: 10.1007/s10712-020-09597-2.

Daniel Labendz. Investigation of schumann resonance polarization parameters. *Journal of atmospheric and solar-terrestrial physics*, 60(18): 1779–1789, 1998.

Gandi Ramarao and Kandasamy Chandrasekaran. Evaluation of an Approximate Channel-Base Current and Its Analytical Function Parameters Based on the Measured Lightning Magnetic Field. *IEEE Transactions on Electromagnetic Compatibility*, 62(1):124–134, 2020. ISSN 1558187X. doi: 10.1109/TEMC.2018.2879541.

J. L. Bermudez, F. Rachidi, W. Janischewskyj, V. Shostak, M. Rubinstein, D. Pavanello, A. M. Hussein, J. S. Chang, and M. Paolone. Determination of lightning currents from far electromagnetic fields: Effect of a strike object. *Journal of Electrostatics*, 65(5-6 SPEC. ISS.):289–295, 2007. ISSN 03043886. doi: 10.1016/j.elstat.2006.09.007.

Chin Leong Wooi, Zulkurnain Abul-Malek, Mohamad Nur Khairul Hafizi Rohani, Ahmad Muhyiddin Bin Yusof, Syahrun Nizam Md Arshad, and Ali I. Elgayar. Comparison of lightning return stroke channel-base current models with measured lightning current. *Bulletin of Electrical Engineering and Informatics*, 8(4):1478–1488, 2019. ISSN 23029285. doi: 10.11591/eei.v8i4.1613.

Silvério Visacro, Amilton Soares, Marco Aurélio O. Schroeder, Luiz C.L. Cherchiglia, and Vander José de Sousa. Statistical analysis of lightning current parameters: Measurements at Morro do Cachimbo station. *Journal of Geophysical Research: Atmospheres*, 109(1):1–11, 2004. ISSN 01480227. doi: 10.1029/2003jd003662.

Nikolay N. Slyunyaev, Evgeny A. Mareev, Vladimir A. Rakov, and Georgy S. Golitsyn. Statistical Distributions of Lightning Peak Currents: Why Do They Appear to Be Lognormal? *Journal of Geophysical Research: Atmospheres*, 123(10):5070–5089, 2018. ISSN 21698996. doi: 10.1029/2017JD028248.

Arthur C. Almeida, Brígida R.P. Rocha, José Ricardo S. Souza, José Alberto S. Sá, and José A.Pissolato Filho. Cloud-to-ground lightning observations over the eastern Amazon Region. *Atmospheric Research*, 117: 86–90, 2012. ISSN 01698095. doi: 10.1016/j.atmosres.2011.08.015.

Alfred B. Chen, Cheng Ling Kuo, Yi Jen Lee, Han Tzong Su, Rue Ron Hsu, Jyh Long Chern, Harald U. Frey, Stephen B. Mende, Yukihiro Takahashi, Hiroshi Fukunishi, Yeou Shin Chang, Tie Yue Liu, and Lou Chuang Lee. Global distributions and occurrence rates of transient luminous events. *Journal of Geophysical Research: Space Physics*, 113(8):1–8, 2008. ISSN 21699402. doi: 10.1029/2008JA013101.

J. Jerauld, V. A. Rakov, M. A. Uman, K. J. Rambo, D. M. Jordan, Ken L. Cummins, and J. A. Cramer. An evaluation of the performance characteristics of the U.S. national lightning detection network in Florida using rocket-triggered lightning. *Journal of Geophysical Research D: Atmospheres*, 110(19):1–16, 2005. ISSN 01480227. doi: 10.1029/2005JD005924.

S. Soula, E. Defer, M. Füllekrug, O. van Der Velde, J. Montanya, O. Bousquet, J. Mlynarczyk, S. Coquillat, J. P. Pinty, W. Rison, P. R. Krehbiel, R. Thomas, and S. Pedeboy. Time and space correlation between sprites and their parent lightning flashes for a thunderstorm observed during the HyMeX campaign. *Journal of Geophysical Research*, 120(22): 11,552–11,574, 2015. ISSN 21562202. doi: 10.1002/2015JD023894.

David Brandwood. *Fourier Transforms in Radar and Signal Processing*. 2013. ISBN 9789896540821.

F. Heidler and J. Cvetić. A class of analytical functions to study the lightning effects associated with the current front. *European Transactions on Electrical Power*, 12(2):141–150, 2002. ISSN 15463109. doi: 10.1002/etep.4450120209.

Daniel C. Bowman and Jonathan M. Lees. The hilbert-huang transform: A high resolution spectral method for nonlinear and nonstationary time series. *Seismological Research Letters*, 84(6):1074–1080, 2013. ISSN 08950695. doi: 10.1785/0220130025.

François Husson, Sébastien Lê, and Jérôme Pagès. *Exploratory multivariate analysis by example using R*. 2010. ISBN 9781439835814. doi: 10.1201/b10345.

Stuart P. Lloyd. Least Squares Quantization in PCM. *IEEE Transactions on Information Theory*, 28(2):129–137, 1982. ISSN 15579654. doi: 10.1109/TIT.1982.1056489.

Sang-Woon Kim and Joon-Min Gil. Research paper classification systems based on tf-idf and lda schemes. *Human-centric Computing and Information Sciences*, 9, 12 2019. doi: 10.1186/s13673-019-0192-7.

Catalin Stoean, Ruxandra Stoean, Roberto Antonio Becerra-García, Rodolfo García-Bermúdez, Miguel Atencia, Francisco García-Lagos, Luis Velázquez-Pérez, and Gonzalo Joya. Unsupervised learning as a complement to convolutional neural network classification in the analysis of saccadic eye movement in spino-cerebellar ataxia type 2. In Ignacio Rojas, Gonzalo Joya, and Andreu Catala, editors, *Advances in Computational Intelligence*, pages 26–37, Cham, 2019. Springer International Publishing.

Javier Herrera-Murcia, Camilo Younes-Velosa, and Leonardo Porras. Variation of lightning peak current parameter as a function of cloud-to-ground lightning flash density in Colombia. *2017 International Symposium on Lightning Protection, XIV SIPDA 2017*, (October):336–340, 2017. doi: 10.1109/SIPDA.2017.8116948.

M. M. Salut, M. B. Cohen, M. A.M. Ali, K. L. Graf, B. R.T. Cotts, and Sushil Kumar. On the relationship between lightning peak current and Early VLF perturbations. *Journal of Geophysical Research: Space Physics*, 118 (11):7272–7282, 2013. ISSN 21699402. doi: 10.1002/2013JA019087.

N.S. Arshad, M. Abdullah, S.A. Samad, and N. Abdullah. High intensity lightning recognition system using Very Low Frequency signal features. *Journal of Atmospheric and Solar-Terrestrial Physics*, page 105520, 2020.

ISSN 13646826. doi: 10.1016/j.jastp.2020.105520.

Fridolin H. Heidler and Christian Paul. High-Speed Video Observation, Currents, and EM-Fields From Four Negative Upward Lightning to the Peissenberg Tower, Germany. *IEEE Transactions on Electromagnetic Compatibility*, pages 1–8, 2020. ISSN 1558187X. doi: 10.1109/TEMC.2020.3032781.

Ting Wu, Daohong Wang, and Nobuyuki Takagi. Upward Negative Leaders in Positive Upward Lightning in Winter: Propagation Velocities, Electric Field Change Waveforms, and Triggering Mechanism. *Journal of Geophysical Research: Atmospheres*, 125(16):1–17, 2020. ISSN 21698996. doi: 10.1029/2020JD032851.

Andrea Pizzuti, Jonathan M. Wilkinson, Serge Soula, Janusz Mlynarczyk, Ivana Kolmašová, Ondej Santolík, Robert Scovell, Alec Bennett, and Martin Füllekrug. Signatures of large peak current lightning strokes during an unusually intense sprite-producing thunderstorm in southern England. *Atmospheric Research*, 249, 2021. ISSN 01698095. doi: 10.1016/j.atmosres.2020.105357.

Robert Boldi, Earle Williams, and Anirban Guha. Determination of the Global-Average Charge Moment of a Lightning Flash Using Schumann Resonances and the LIS/OTD Lightning Data. *Journal of Geophysical Research: Atmospheres*, 123(1):108–123, 2018. ISSN 21698996. doi: 10.1002/2017JD027050.

E. Prácser, T. Bozóki, G. Sátori, E. Williams, A. Guha, and H. Yu. Reconstruction of Global Lightning Activity Based on Schumann Resonance Measurements: Model Description and Synthetic Tests. *Radio Science*, 54(3):254–267, 2019. ISSN 1944799X. doi: 10.1029/2018RS006772.

Erno Pracser, Tamas Bozoki, Gabriella Satori, Janos Takatsy, Earle Williams, and Anirban Guha. Two Approaches for Modeling ELF Wave Propagation in the Earth-Ionosphere Cavity with Day-Night Asymmetry. *IEEE Transactions on Antennas and Propagation*, (5):1–7, 2020. ISSN 15582221. doi: 10.1109/TAP.2020.3044669.

Toshio Ogawa and Masayuki Komatsu. Analysis of q burst waveforms. *Radio Science*, 42(1):1–11, 2007. ISSN 00486604. doi: 10.1029/2006RS003493.

Graphical Abstract

Segmentation and characteristic extraction for Schumann Resonance transient events